CrystEngComm

ROYAL SOCIETY OF CHEMISTRY

COMMUNICATION

View Article Online
View Journal | View Issue

Cite this: *CrystEngComm*, 2021, **23**, 6490

Received 14th June 2021,
Accepted 15th August 2021

DOI: 10.1039/d1ce00790d

rsc.li/crystengcomm

In situ reconstruction of ZIF-8 loaded on fibrous supports†

Leilei Song,[abc] Siqi Li[a] and Tao Li *[a]

A simple solution casting technique was developed to load ZIF-8 particles on three commercially available fibrous supports. Benefiting from the open structure and high surface area of these fibrous networks, ZIF-8 particles can undergo a full cycle of degradation and recrystallization in a vapor-phase with 46% of their porosity recovered in the end.

Metal–organic frameworks (MOFs) have risen to be a central theme in the field of porous materials as well as materials science in general.[1–3] Their highly crystalline framework, high surface area and tunable pore chemistry hold promise for various applications such as gas storage, separation, catalysis, drug delivery, sensing, and more.[4–15]

At present, MOF materials prepared at the lab scale mostly exist as microcrystalline powders. The irregular shape, fine grain size and the lack of mechanical strength of powders make them difficult to be directly used in industrial applications.[16–18] Therefore, finding a low-cost process for structuring MOF materials into pellets, sheets or other shapes is a critical step and a timely requirement toward their industrial deployment. On the other hand, MOFs are widely criticized for their lack of chemical stability. When used as sorbent materials, how to handle chemically degraded MOFs, particularly in their shaped form, is a critical aspect that needs to be properly addressed.

Compared to zeolites which are routinely structured into pellets or monoliths through granulation or pelletization,[19,20] MOF structuring meets new challenges. Due to the poor mechanical properties of many MOFs, traditional pelletization and extrusion processes that rely on excessive external forces often cause irreversible damage to the crystallinity of MOFs thereby lowering their inherent porosity.[18,21,22] Alternatively, MOFs can be mixed with polymer binders to form MOF–polymer composites of specific shapes.[23–28] However, random mixing of polymers and MOF particles often leads to pore blocking thereby rendering a part of the MOF pores inaccessible by guest molecules.[26,29,30] In addition, several groups have also shown that MOFs can be grown onto pre-shaped polymer substrates.[31–34] However, high MOF loading is difficult to achieve through this method. Meanwhile, the multistep process also increases cost and complicates the production.

Fibrous materials are excellent supports for powders due to several reasons. First, there is a rich library of fibrous materials ranging from natural to synthetic fibres to meet the needs of various applications. Meanwhile, fibres with adjustable thickness and porosity can be easily obtained through technological means such as weaving, melt blowing, electrospinning, *etc.*[35–37] The intertwined network of fibres can spatially separate and compartmentalize porous particles allowing more efficient guest diffusion. In addition, the excellent mechanical properties of fibres allow maximum processability which can compensate the rigidity of powdery materials when made into composites. Based on these attributes, we hypothesize that the high surface area of the fibres can also make them an excellent host for chemically

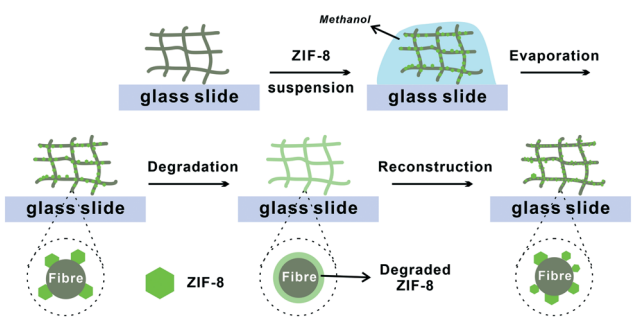

Fig. 1 Schematic illustration of the degradation–reconstruction process of ZIF-8 loaded on various fibres.

[a] *School of Physical Science and Technology, ShanghaiTech University, 201210 Shanghai, People's Republic of China. E-mail: litao1@shanghaitech.edu.cn*
[b] *Shanghai Advanced Research Institute, Chinese Academy of Sciences, 201203, Shanghai, People's Republic of China*
[c] *University of Chinese Academy of Sciences, Beijing 100049, People's Republic of China*

† Electronic supplementary information (ESI) available. See DOI: 10.1039/d1ce00790d

degraded MOFs. The open fibrous network will further allow vapor-phase reconstruction of the MOFs back to their crystalline state. There have been quite a few reports about using fibres as MOF supports which either grow the MOF directly on the fibre or electrospin the MOF/polymer mixture into fibres.[38–40] These methods, although promising, are difficult to be used in large scale manufacturing.

Here, we report a facile method to construct MOF–fibre composites. We selected two natural fibrous materials, cotton fabric and filter paper, and one mineral fibre, rockwool, as supporting matrices for zeolitic imidazolate framework-8 (ZIF-8) (Fig. 1). ZIF-8 is an iconic MOF that has showed tremendous potential as a fuel cell membrane and gas separation membrane.[41–45] Utilizing the hydrophilicity and capillary action of these fibres, ZIF-8 can be easily loaded onto the support through a simple solution casting step thereby achieving 29–40 wt% loading capacity (Table S1†). The loaded ZIF-8 particles adhered to the surfaces of the fibres and fully retained their sorption properties. More impressively, after degradation of ZIF-8 using acid vapor, the metal ion and ligand precursors were evenly coated on the fibre surfaces which can later be recrystallized back to its crystalline form through an *in situ* vapor-assisted reconstruction step resulting in a recovery of half of its original N_2 adsorption capacity.

To begin with, we selected a widely popular MOF, ZIF-8,[41] as a model system for this study. Uniform ZIF-8 particles with sizes of 900 ± 50 nm and 15 ± 5 μm were synthesized according to the reported method (Fig. S1†).[46] The powder X-ray diffraction pattern showed highly matched diffraction peaks between the as-synthesized ZIF-8 and the simulated pattern suggesting good crystallinity (Fig. S2†). For the support, two natural fibrous materials, cotton fabric and filter paper, and one mineral fibre, rockwool (commonly used as a growth medium in hydroponic farming), were selected for this study.

These fibres are all hydrophilic and water absorbent due to the abundance of hydroxyl groups. The hydrophilicity of the fibrous-support creates capillary action and helps ZIF-8 particles evenly disperse in the support. Moreover, the polar functional groups presented on the fiber can serve as the nucleation centres during the latter ZIF-8 reconstruction step. These fabrics were cut into samples of 2 × 2 cm and spread onto a glass slide. The scanning electron microscopy (SEM) images showed that the diameters of the fibres for cotton, filter paper and rockwool are mostly within the range of 5–20 μm (Fig. 2A, C and S4A†). The porosities of these three fibrous materials are estimated to be 4.4, 2.3 and 12.5 cc g^{-1} (see the ESI†). To load ZIF-8 particles onto these supports, a prescribed amount of 120 mg ml^{-1} ZIF-8 suspension in methanol was drop casted onto the fibre and was allowed to evaporate naturally at room temperature. This process was repeated 2–3 times to obtain the final composites, namely ZIF-8⊂cotton, ZIF-8⊂filter, and ZIF-8⊂rockwool. In principle, the MOF loading capacity is only limited by the porosity of the fibrous support. The SEM images clearly showed that ZIF-8 was occupying the gaps in between fibres in all three

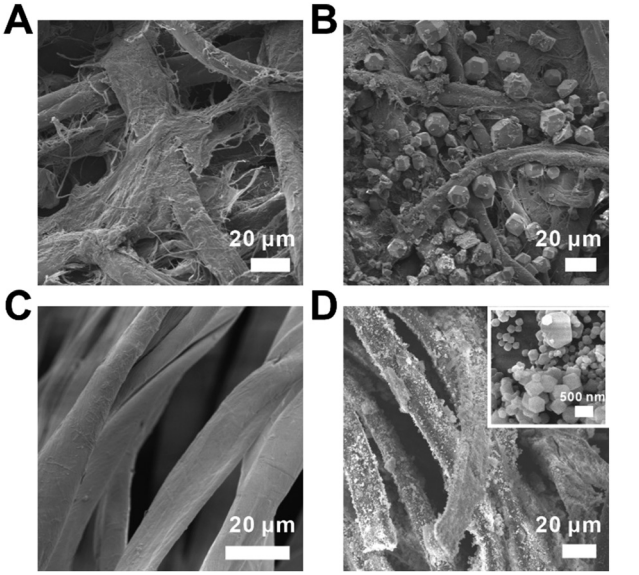

Fig. 2 SEM images of the (A) filter paper, (B) ZIF-8⊂filter, (C) cotton fabric, and (D) ZIF-8⊂cotton (the inset is a close-up image of the ZIF-8 particle on the fibre surface).

samples (Fig. 2B, D and S4B†). The PXRD patterns revealed that these composites exhibited identical diffraction peaks as those of the as-synthesized ZIF-8 suggesting that the crystallinity was well preserved in their respective composites (Fig. 3A and S5†).

Next, to demonstrate the benefit of the fibre supported MOF, we turned to explore the degradation–reconstruction process of ZIF-8 on the fibres. A previous study by Majano *et al.* has shown that certain MOFs can be recrystallized through solvent vapor treatment after degradation.[47] However, in most cases, the morphology of the MOF particles was changed. The presence of fibrous supports spatially separates MOF particles and therefore may lead to a higher recrystallization rate. To demonstrate this hypothesis, first, a piece of a ZIF-8⊂cotton sample was placed in a container exposed to acetic acid vapor at room temperature for 1 h. During this process, ZIF-8 particles gradually degraded into Zn^{2+} ions and 2-methylimidazole (2-MIM). We denote this sample as ZIF-8⊂cotton-DE. Similarly, ZIF-8⊂rockwool-DE and ZIF-8⊂filter-DE were also prepared using the same protocol. The PXRD patterns of ZIF-8⊂cotton-DE, ZIF-8⊂rockwool-DE and ZIF-8⊂filter-DE showed that the characteristic diffraction peaks of ZIF-8 disappeared after acid treatment indicating complete degradation of ZIF-8 (Fig. 3A and S5†). SEM images also confirmed that the fibres were visibly coated by a layer of ZIF-8 precursors (Fig. 3B, D and S6A†). Taking ZIF-8⊂filter-DE as an example, the energy dispersion X-ray spectroscopy (EDS) mapping showed that the two characteristic elements, Zn and N, from ZIF-8 were distributed mainly on the surface of the filter paper fibre (Fig. 3C). This evidence confirms that the decomposition products of ZIF-8 were retained on the surfaces of the fibres.

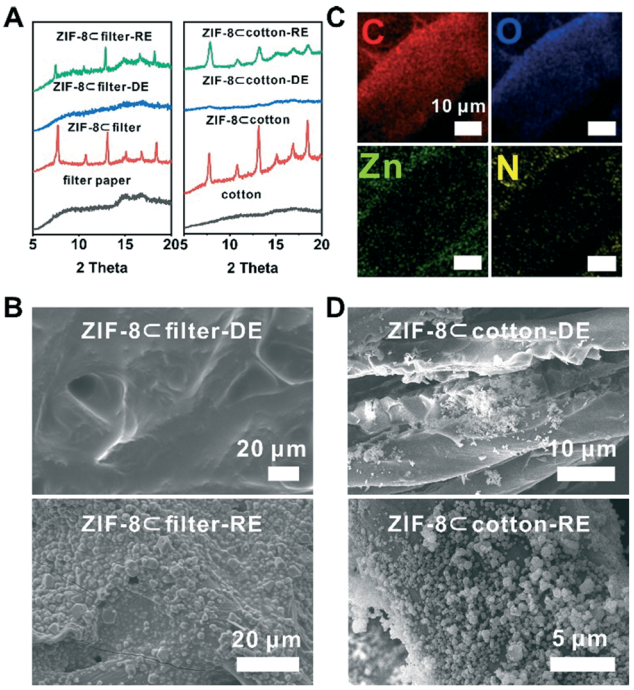

Fig. 3 (A) PXRD patterns of the degradation–reconstruction processes of ZIF-8 ⊂filter and ZIF-8⊂cotton; SEM images of (B) ZIF-8⊂filter after degradation and reconstruction and (D) ZIF-8⊂cotton after degradation and reconstruction; (C) EDS elemental mapping images of ZIF-8⊂filter after degradation.

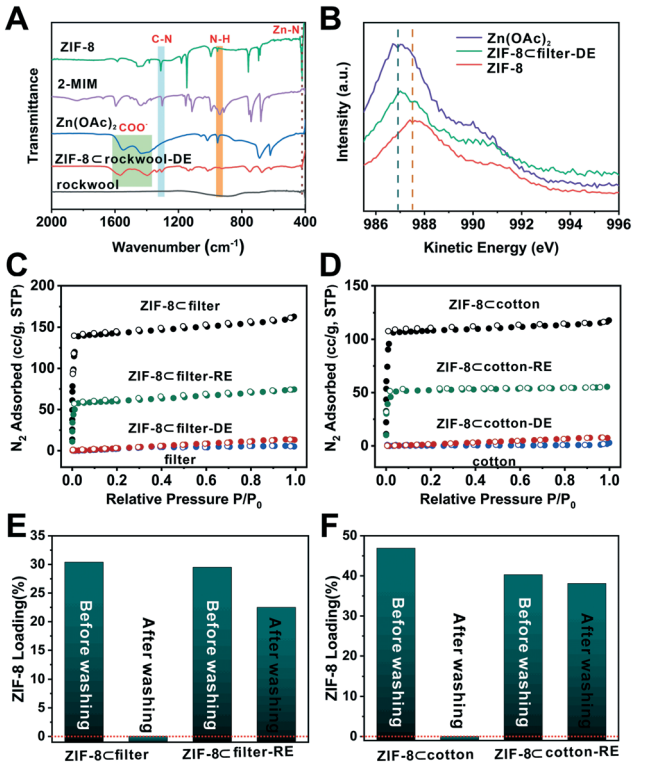

Fig. 4 (A) The FTIR spectrum of ZIF-8, 2-MIM, $Zn(OAc)_2$, ZIF-8⊂rockwool-DE and rockwool. (B) The Zn LMM Auger spectrum of $Zn(OAc)_2$, ZIF⊂filter-DE and ZIF-8; 77 K N_2 sorption isotherms of (C) ZIF-8⊂filter and (D) ZIF-8⊂cotton during the degradation–reconstruction cycle; ZIF-8 loading of (E) ZIF-8⊂filter and ZIF-8⊂filter-RE before and after washing and (F) ZIF-8⊂cotton and ZIF-8⊂cotton-RE before and after washing.

To better understand the chemistry behind the degradation process, Fourier-transform infrared (FTIR) spectroscopy was used to analyze these samples. $Zn(OAc)_2$ showed a series of COO^- bands at 1400 and 1550–1650 cm^{-1} (Fig. 4A). For 2-methylimidazole, the absorption peaks were located at 1303 and 945 cm^{-1} which correlate to the C–N stretching and N–H bending, respectively. Moreover, the peak at 421 cm^{-1} can be ascribed to the Zn–N stretching.[48] Compared to these standard samples, the N–H bending and Zn–N stretching peaks disappeared in the IR spectra of ZIF-8⊂rockwool-DE. Meanwhile, the COO^- signal reappeared. This suggests that Zn^{2+} primarily occurred in the form of $Zn(OAc)_2$ after degradation. Meanwhile, 2-MIM was likely to be protonated. We further used XPS and Auger spectroscopy to analyze $Zn(OAc)_2$, ZIF-8 and ZIF-8⊂rockwool-DE to further probe the chemical nature of the degraded ZIF-8. Since Zn can only exist as Zn^{2+} here, the Zn^{2+} peak in the Zn LMM Auger spectrum of ZIF-8⊂rockwool-DE deviated from that of ZIF-8 and shifted towards that of $Zn(OAc)_2$. This indicates that ZIF-8 was degraded into $Zn(OAc)_2$ and 2-methylimidazole (Fig. 4B). We further proceeded to analyse the Zn^{2+} chemical environment using X-ray photoelectric spectroscopy (XPS) and Auger spectroscopy. The Zn LMM Auger peaks in $Zn(OAc)_2$ and ZIF-8 were located at 986.9 eV and 987.5 eV. In contrast, the Zn peak in ZIF-8⊂filter-DE, however, manifests a linear combination of those of $Zn(OAc)_2$ and ZIF-8 with $Zn(OAc)_2$ as the dominant phase (Fig. 4B). This again confirmed the near complete degradation of ZIF-8 to $Zn(OAc)_2$ after HOAc vapor treatment.

In situ vapor-assistant reconstruction was then carried out aiming to recrystallize Zn^{2+} and 2-MIM back into ZIF-8. Specifically, ZIF-8⊂cotton-DE, ZIF-8⊂filter-DE, and ZIF-8⊂rockwool-DE samples were again placed in a sealed chamber along with a small amount of methanol (Fig. S7†). The chamber was heated to 70 °C for 24 h to obtain reconstructed samples which are denoted as ZIF-8⊂cotton-RE, ZIF-8⊂filter-RE, and ZIF-8⊂rockwool-RE, respectively. The PXRD patterns of the three reconstructed samples all showed characteristic peaks of ZIF-8 suggesting the successful recovery of ZIF-8 (Fig. 3A and S4†). The SEM images revealed that crystalline particles with a ZIF-8-like morphology reappeared on the surfaces of fibres in all three cases (Fig. 3B, D and S5B†). A N_2 adsorption experiment was then carried out to quantitatively evaluate the loss and recovery of ZIF-8 porosity after the degradation and reconstruction process. As shown in Fig. 4C, after acid vapor degradation, the N_2 absorption capacity decreased from 164 cc g^{-1} for ZIF-8⊂filter to 5 cc g^{-1} (P/P_o = 0.95) for ZIF-8⊂filter -DE indicating the complete loss of porosity. After vapor-assisted reconstruction, the N_2 uptake capacity of ZIF-8⊂filter -RE returned to 75 cc g^{-1} which accounts for 46% of the uptake value of ZIF-8⊂cotton (164 cc g^{-1}) (Fig. 4C). Similarly, ZIF-8⊂cotton exhibited a N_2 uptake capacity of 118 cc g^{-1} (77

K, P/P_o = 0.95). After acid vapor treatment, ZIF-8⊂cotton-DE exhibited an uptake capacity of only 6 cc g^{-1}. ZIF-8⊂cotton-RE, however, showed a N_2 uptake capacity of 55 cc g^{-1}, which accounts for 46% of the N_2 adsorption capacity of ZIF-8⊂cotton (Fig. 4D).

Lastly, the attrition resistance of these fibre-supported MOF composites was investigated. Specifically, we soaked ZIF-8⊂filter and ZIF-8⊂filter-RE (~8 × 8 mm in size) in an excess of methanol (~4 ml) and the samples were agitated on the rotator for 20 min. Then, SEM and TGA were used to characterize and quantify the amount of MOFs retained after washing. The SEM images showed that the washing step removed most of the ZIF-8 particles from ZIF-8⊂filter (Fig. 4E , S8A and S10A†). Interestingly, after 1 cycle of degradation–reconstruction, the ZIF-8 particles became more attrition resistant as can be seen from the SEM images of ZIF-8⊂filter-RE after washing (Fig. S8B†). TGA analysis showed that more than 79% of the ZIF-8 particles were retained after washing. It is clear that the reconstruction step forced the newly formed ZIF-8 particles to firmly attach to the surface of the fibres thereby increasing their attrition resistance. Similar results were also obtained for ZIF-8⊂cotton and ZIF-8⊂cotton-RE (Fig. 4F, S9 and S10B†).

In summary, we demonstrated a simple solution casting approach for the preparation of three ZIF-8-loaded fibrous composites. The ZIF-8 particles confined among the fibres fully retained their crystallinity and sorption properties. We further demonstrated that the fibre loaded ZIF-8 could be recrystallized back to its crystalline state through a vapor-assisted reconstruction step with near half of the N_2 uptake recovery rate. These results exemplify that supporting MOFs with fibrous materials is a viable option for structuring MOF materials and to extend the longevity of MOF materials under realistic environments through vapor-assisted reconstruction.

This work was supported by the National Natural Science Foundation of China (Grant No. 22075181). The authors thank the support from the Analytical Instrumentation Center (Grant No. SPSTAIC10112914) and the Centre for High-resolution Electron Microscopy (ChEM) of SPST at ShanghaiTech University under Grant No. EM02161943.

Conflicts of interest

There are no conflicts to declare.

Notes and references

1 H. Furukawa, K. E. Cordova, M. O'Keeffe and O. M. Yaghi, *Science*, 2013, **341**, 1230444.
2 H. C. Zhou and S. Kitagawa, *Chem. Soc. Rev.*, 2014, **43**, 5415–5418.
3 G. Maurin, C. Serre, A. Cooper and G. Férey, *Chem. Soc. Rev.*, 2017, **46**, 3104–3107.
4 J.-R. Li, R. J. Kuppler and H.-C. Zhou, *Chem. Soc. Rev.*, 2009, **38**, 1477.
5 Y. He, W. Zhou, G. Qian and B. Chen, *Chem. Soc. Rev.*, 2014, **43**, 5657–5678.
6 K. Sumida, D. L. Rogow, J. A. Mason, T. M. McDonald, E. D. Bloch, Z. R. Herm, T.-H. Bae and J. R. Long, *Chem. Rev.*, 2012, **112**, 724–781.
7 N. C. Burtch, H. Jasuja and K. S. Walton, *Chem. Rev.*, 2014, **114**, 10575–10612.
8 J. Lee, O. K. Farha, J. Roberts, K. A. Scheidt, S. T. Nguyen and J. T. Hupp, *Chem. Soc. Rev.*, 2009, **38**, 1450.
9 P. Horcajada, T. Chalati, C. Serre, B. Gillet, C. Sebrie, T. Baati, J. F. Eubank, D. Heurtaux, P. Clayette, C. Kreuz, J.-S. Chang, Y. K. Hwang, V. Marsaud, P.-N. Bories, L. Cynober, S. Gil, G. Férey, P. Couvreur and R. Gref, *Nat. Mater.*, 2010, **9**, 172–178.
10 P. Horcajada, R. Gref, T. Baati, P. K. Allan, G. Maurin, P. Couvreur, G. Férey, R. E. Morris and C. Serre, *Chem. Rev.*, 2012, **112**, 1232–1268.
11 J.-D. Xiao and H.-L. Jiang, *Acc. Chem. Res.*, 2019, **52**, 356–366.
12 M.-X. Wu and Y.-W. Yang, *Adv. Mater.*, 2017, **29**, 1606134.
13 L. S. Xie, G. Skorupskii and M. Dincă, *Chem. Rev.*, 2020, **120**, 8536–8580.
14 L. E. Kreno, K. Leong, O. K. Farha, M. Allendorf, R. P. Van Duyne and J. T. Hupp, *Chem. Rev.*, 2012, **112**, 1105–1125.
15 M.-F. Wang, Y. Mi, F.-L. Hu, Z. Niu, X.-H. Yin, Q. Huang, H.-F. Wang and J.-P. Lang, *J. Am. Chem. Soc.*, 2020, **142**, 700–704.
16 X.-M. Liu, L.-H. Xie and Y. Wu, *Inorg. Chem. Front.*, 2020, **7**, 2840–2866.
17 M. Rubio-Martinez, C. Avci-Camur, A. W. Thornton, I. Imaz, D. Maspoch and M. R. Hill, *Chem. Soc. Rev.*, 2017, **46**, 3453–3480.
18 B. Valizadeh, T. N. Nguyen and K. C. Stylianou, *Polyhedron*, 2018, **145**, 1–15.
19 S. Mitchell, N. L. Michels and J. Perez-Ramirez, *Chem. Soc. Rev.*, 2013, **42**, 6094–6112.
20 W. Schwieger, A. G. Machoke, T. Weissenberger, A. Inayat, T. Selvam, M. Klumpp and A. Inayat, *Chem. Soc. Rev.*, 2016, **45**, 3353–3376.
21 J. Ren, N. M. Musyoka, H. W. Langmi, A. Swartbooi, B. C. North and M. Mathe, *Int. J. Hydrogen Energy*, 2015, **40**, 4617–4622.
22 T. Tian, Z. Zeng, D. Vulpe, M. E. Casco, G. Divitini, P. A. Midgley, J. Silvestre-Albero, J.-C. Tan, P. Z. Moghadam and D. Fairen-Jimenez, *Nat. Mater.*, 2018, **17**, 174–179.
23 J. Cousin-Saint-Remi, S. Van Der Perre, T. Segato, M.-P. Delplancke, S. Goderis, H. Terryn, G. Baron and J. Denayer, *ACS Appl. Mater. Interfaces*, 2019, **11**, 13694–13703.
24 A. Mallick, G. Mouchaham, P. M. Bhatt, W. Liang, Y. Belmabkhout, K. Adil, A. Jamal and M. Eddaoudi, *Ind. Eng. Chem. Res.*, 2018, **57**, 16897–16902.
25 H. Zhu, X. Yang, E. D. Cranston and S. Zhu, *Adv. Mater.*, 2016, **28**, 7652–7657.
26 J. C. Moreton, M. S. Denny and S. M. Cohen, *Chem. Commun.*, 2016, **52**, 14376–14379.
27 B. Valizadeh, T. N. Nguyen, B. Smit and K. C. Stylianou, *Adv. Funct. Mater.*, 2018, **28**, 1801596.

28 G. W. Peterson, J. J. Mahle, T. M. Tovar and T. H. Epps, *Adv. Funct. Mater.*, 2020, **30**, 2005517.
29 C. Lu, T. Ben, S. Xu and S. Qiu, *Angew. Chem., Int. Ed.*, 2014, **53**, 6454–6458.
30 A. Sabetghadam, X. Liu, M. Benzaqui, E. Gkaniatsou, A. Orsi, M. M. Lozinska, C. Sicard, T. Johnson, N. Steunou, P. A. Wright, C. Serre, J. Gascon and F. Kapteijn, *Chem. – Eur. J.*, 2018, **24**, 7949–7956.
31 C. Zhang, Y. Li, H. Wang, S. He, Y. Xu, C. Zhong and T. Li, *Chem. Sci.*, 2018, **9**, 5672–5678.
32 L. D. O'Neill, H. Zhang and D. Bradshaw, *J. Mater. Chem.*, 2010, **20**, 5720.
33 A. Centrone, Y. Yang, S. Speakman, L. Bromberg, G. C. Rutledge and T. A. Hatton, *J. Am. Chem. Soc.*, 2010, **132**, 15687–15691.
34 M. L. Pinto, S. Dias and J. Pires, *ACS Appl. Mater. Interfaces*, 2013, **5**, 2360–2363.
35 K. Bilisik, *Text. Res. J.*, 2012, **82**, 725–743.
36 F. Zuo, D. H. Tan, Z. Wang, S. Jeung, C. W. Macosko and F. S. Bates, *ACS Macro Lett.*, 2013, **2**, 301–305.
37 S. Jiang, Y. Chen, G. Duan, C. Mei, A. Greiner and S. Agarwal, *Polym. Chem.*, 2018, **9**, 2685–2720.
38 M. A. Bunge, A. B. Davis, K. N. West, C. W. West and T. G. Glover, *Ind. Eng. Chem. Res.*, 2018, **57**, 9151–9161.
39 D. B. Dwyer, N. Dugan, N. Hoffman, D. J. Cooke, M. G. Hall, T. M. Tovar, W. E. Bernier, J. Decoste, N. L. Pomerantz and W. E. Jones, *ACS Appl. Mater. Interfaces*, 2018, **10**, 34585–34591.
40 Y. Dou, W. Zhang and A. Kaiser, *Adv. Sci.*, 2020, **7**, 1902590.
41 K. S. Park, Z. Ni, A. P. Cote, J. Y. Choi, R. Huang, F. J. Uribe-Romo, H. K. Chae, M. O'Keeffe and O. M. Yaghi, *Proc. Natl. Acad. Sci. U. S. A.*, 2006, **103**, 10186–10191.
42 H. Q. Liang, Y. Guo, Y. Shi, X. Peng, B. Liang and B. Chen, *Angew. Chem.*, 2020, **59**, 7732–7737.
43 Y. Guo, Z. Jiang, W. Ying, L. Chen, Y. Liu, X. Wang, Z.-J. Jiang, B. Chen and X. Peng, *Adv. Mater.*, 2018, **30**, 1705155.
44 H.-Q. Liang, Y. Guo, X. Peng and B. Chen, *J. Mater. Chem. A*, 2020, **8**, 11399–11405.
45 K. Li, D. H. Olson, J. Seidel, T. J. Emge, H. Gong, H. Zeng and J. Li, *J. Am. Chem. Soc.*, 2009, **131**, 10368–10369.
46 C. Zhang, R. P. Lively, K. Zhang, J. R. Johnson, O. Karvan and W. J. Koros, *J. Phys. Chem. Lett.*, 2012, **3**, 2130–2134.
47 G. Majano, O. Martin, M. Hammes, S. Smeets, C. Baerlocher and J. Pérez-Ramírez, *Adv. Funct. Mater.*, 2014, **24**, 3855–3865.
48 Y. Hu, H. Kazemian, S. Rohani, Y. Huang and Y. Song, *Chem. Commun.*, 2011, **47**, 12694.

